CEAI, Vol.24, No.3, pp. 31-39, 2022 Printed in Romania

Model Prediction Hybrid Parallel Direct Speed Control of Permanent Magnet Synchronous Machines for Electric Vehicles

Siyu Gao, Yanjun Wei, Hanhong Qi*, Di Zhang*, Yao Wei

College of Electrical Engineering, Yanshan University, Qinhuangdao 066004 China.
(Tel: 86-335-8058471, e-mail: gaosiyu@stumail.ysu.edu.cn, yjwei@ysu.edu.cn, hhqi@ysu.edu.cn, dzhang1120@ysu.edu.cn*, yao.wei@fjirsm.ac.cn).*

Abstract: Model predictive direct speed control (MP-DSC) has been widely concerned for its unique fast speed response capability and simple structure. However, the control performance of conventional MP-DSC is extremely susceptible to the influence of weight factor in the cost function and external disturbances. In this paper, a model prediction hybrid parallel direct speed control (MP-HPDSC) method is proposed. The composite prediction error cost function is decomposed into independent forms: speed error, torque error and flux error, and the optimal voltage vector (VV) is selected by optimized parallel structure to eliminate the influence of weight factor. Meanwhile, the lumped disturbances including the unmodeled part of the traditional model and the external disturbance are introduced into the system model to improve the anti-disturbance ability and dynamic response ability of the system. Compared with other methods, the proposed MP-HPDSC has faster speed tracking, more stable torque output and anti-disturbance performance, which is more adaptive to the control requirements of electric vehicles system. The stability and effectiveness of the proposed method is verified by simulation and experiment results.

Keywords: PMSM, Weighting factor elimination, Cascade predictive control, Linear extended state observer, Model prediction hybrid parallel direct speed control.

1. INTRODUCTION

Nowadays, with the vigorous promotion of clean energy, electric vehicles (EVs) have attracted the research enthusiasm of a large number of scholars due to their characteristics of clean energy, high efficiency and low noise (Liu et al., 2016). This also greatly promoted the development of the control method of permanent magnet synchronous machines (PMSM) as the main driving unit of EVs. On the basis of traditional control methods (vector control (VC) and direct torque control (DTC)), many effective and innovative control methods have been proposed (Casadei et al., 2002; Navardi et al., 2018).

The complex operation environment of electric vehicle brings more requirements for machine control, such as fast speed tracking ability, stable torque output and strong disturbance ability (Vafamand et al., 2019; Li et al., 2019; Huang et al., 2021). The MP-DSC has advantages of intuitive concept and simple implementation, and is regarded as a superior alternative to conventional control methods (Preindl et al., 2013). And the MP-DSC control structure is more concise by omitting the speed loop controller, with ultra-fast speed response ability (Wakodikar et al., 2020). However, conventional MP-DSC still faces some problems such as difficult adjustment of weighting factor and weak resistance to external disturbance. In order to enhance the resistance of the system to external disturbance, many excellent control algorithms have been proposed, such as Kalman filter method (Mwasilu et al., 2017), backstepping method (Sun et al., 2019; Uddin et al., 2019), adaptive observer (Wang et al., 2020b), sliding mode observer (Zhang et al., 2019a), model reference adaptive method (Jabbour et al., 2019), and so on. Zhang et al. used the sliding mode observer to improve the anti-disturbance ability of the system, and optimized the cost function simultaneously, avoiding the process of balancing the importance degree between different state quantities by weighting factors (Zhang et al., 2019a). Similarly, the model reference adaptive method is combined with the fuzzy control method to improve the anti-disturbance ability of the system, and the fuzzy logic is used to dynamically adjust the weighting factor so that the system can show excellent response performance under different working conditions (Jabbour et al., 2019). However, this complex and efficient control method obviously increases the computational burden of the system and the number of parameters to be designed.

The complex cost function composed of a variety of constraints is faced with the difficulty of weighting factor tuning. By analyzing the influence of different weighting factor combinations on the control performance, it is concluded that the weighting factor combination determined by the ratio of rated torque to flux linkage is not optimal (Zhang et al., 2016). Therefore, effectively eliminating the influence of weighting factors for control performance is an urgent problem to be solved (Guazzelli et al., 2019; Caseiro et al., 2019).

A non-dominated sorting genetic algorithm was used to obtain the relationship between the response performance of torque and flux and the switching frequency, so as to determine the appropriate weighting factor combination method was proposed in (Guazzelli et al., 2019). The dynamic weighting factor real-time adjustment analysis technique gives a new idea for adjusting the combination of weighting factors, and the redefined cost function makes the design of weighting factors more intuitive (Caseiro et al., 2019). Intelligent control and adaptive methods can achieve good response performance, and effectively eliminate the influence of the weighting factor, but they need a lot of experimental data to support, which affects the portability of the control method. In addition, many control strategies abandon the weighting factor in the cost function to avoid the tedious tunning process. The predictive torque error control item is integrated into the predictive flux error control item through some transformation methods (Wu et al., 2018; Zhang et al., 2015). However, the number of constraints in this method is limited, which is not conducive to expanding the number of constraints in the cost function.

It is an effective solution to eliminate the weighting factor by optimizing the structure of cost function. The composite cost function is decomposed into the cost function composed of a single prediction error control term, and then the sequence prediction optimization structure is constructed by multiple single cost functions, so as to gradually reduce the number of candidate voltage vectors (VVs) until the optimal one is obtained (Zhang et al., 2019b). The generalized sequential predictive torque control (SPTC) proposed in (Zhang et al., 2019b), eight VVs are reduced to three through the first cost function, and the optimal VV is selected from the reduced VVs through the second cost function. Furthermore, parallel predictive torque control (PPTC) is proposed in (Wang et al., 2020a; Xie et al., 2021), which synchronously evaluates and clusters all VVs according to independent cost functions and boundary conditions, and selects the optimal VV according to the classification results. Similarly, the improved PPTC proposed in (Xie et al., 2020) also considers the influence of parameter mismatch and designs a parameter observer to improve the anti-interference capability of the system.

Hence, in order to solve the problems existing in MP-DSC, a model prediction hybrid parallel direct speed control method is proposed in this paper, which can effectively eliminate the weighting factor and improve the anti-interference performance. Firstly, a parallel predictive control structure is proposed for speed, torque and flux predictive error control terms to eliminate the weighting factor. Secondly, the optimized parallel predictive control structure reduces the dynamic adjustment process for multiple control objectives, and the determination of the optimal VV is more reasonable and accurate. Finally, the CPTC(Garcia et al., 2016) method based on linear extended state observer (LESO)(Gao, 2015)is proposed to ensure the fast response ability and greatly improve the robustness of the system. Meanwhile, the designed LESO only needs to design one parameter, which provides convenience for parameter tunning.

Table 1. Noun abbreviation.

CPTC	Cascade predictive torque control
CVVM	Candidate voltage vector matrix
LESO	Linear extended state observer
MP-HPDSC	Model prediction hybrid parallel direct speed control
MP-DSC	Model predictive direct speed control
PPTC	Parallel predictive torque control
THD	Total Harmonic Distortion
VV	Voltage vector

This paper is structured as follows. In Section 2, the mathematical model of the SPMSM and the principle of conventional MP-DSC is presented. In Section 3, the proposed MP-HPDSC algorithm is introduced. In Section 4 and 5, the comparison of simulation and experimental results of MP-DSC method, PPTC method and proposed MP-HPDSC method is provided. Finally, this paper is concluded in Section 6.

2. MODEL OF SPMSM AND CONVENTIONAL MP-DSC

2.1 Mathematical Model of SPMSM

The voltage equation of SPMSM on dq axis is as follows: (Rodriguez et al., 2012):

$$\begin{cases} u_d = R_s i_d + L_s \frac{d}{dt} i_d - p\omega_m L_s i_q \\ u_q = R_s i_q + L_s \frac{d}{dt} i_q + p\omega_m L_s i_d + p\omega_m \psi_f \end{cases} \tag{1}$$

where u_d and u_q represent the stator voltages as input; i_d and i_q represent the stator currents as output; L_s, R_s and p represent the stator inductance, stator resistance and number of pole pair; ω_m represents the mechanical angular velocity;

The torque and stator flux equations of SPMSM on dq axis are as follows:

$$T_e = 1.5p\psi_f i_q = K_t i_q \tag{2}$$

$$\begin{cases} \psi_d = L_s i_d + \psi_f \\ \psi_q = L_s i_q \end{cases} \tag{3}$$

where ψ_d and ψ_q represent the stator flux linkages; T_e represents the torque; ψ_f represent the rotor flux linkage; The stator current is input, torque and flux are output.

The speed equation of SPMSM on dq axis is shown as follows:

$$\frac{d}{dt}\omega_m = \frac{1}{J}T_e - \frac{1}{J}T_l - \frac{B}{J}\omega_m \tag{4}$$

where T_l represent the load torque respectively; the parameters B and J represent the viscous friction coefficient and rotor inertia respectively; The torque is input, speed is output.

2.2 Conventional MP-DSC Strategy

The control block diagram of conventional MP-DSC method is shown in Fig. 1(Preindl et al., 2013). The control process of conventional MP-DSC mainly includes the prediction of speed and current, and the selection of optimal voltage vector.

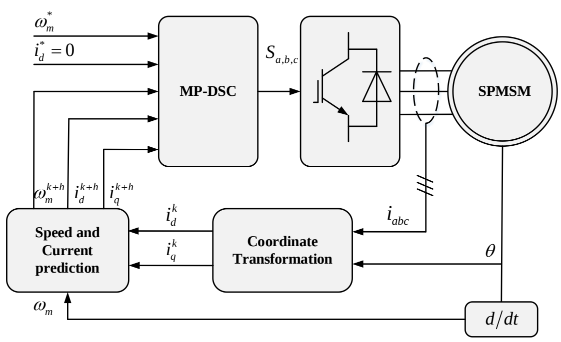

Fig. 1. Control block diagram of MP-DSC.

The first-order Euler discretization method is used to discretize equations (1) and (4), and the prediction equations of current and speed can be obtained as follows:

$$\begin{cases} i_d^{k+1} = i_d^k + \frac{h}{L_s}\left(u_d^k - R_s i_d^k + p\omega_m L_s i_q^k\right) \\ i_q^{k+1} = i_q^k + \frac{h}{L_s}\left(u_q^k - R_s i_q^k - p\omega_m L_s i_d^k - p\omega_m \psi_f\right) \end{cases} \tag{5}$$

$$\omega_m^{k+1} = \left(1 - h\frac{B}{J}\right)\omega_m^k + \frac{h}{J}\left(K_t i_q^{k+1} - \hat{T}_l^k\right) \tag{6}$$

where i_d^{k+1} and i_q^{k+1} represent the current predicted values; ω_m^{k+1} represents the speed predicted value; $\hat{T}_l^k$ is the estimation of load torque at kth time; h is the sampling period.

The optimal voltage vector selection of conventional MP-DSC is realized by using traditional compound cost function. The cost function in the conventional MP-DSC is defined as follows:

$$g = \sum_{n=1}^{N}\left[Q_\omega * (\omega_m^{k+n} - \omega_m^*)^2 + Q_A * c_A^{k+n} + Q_L * c_L^{k+n}\right]$$

where the first term in the cost function is the speed control term, and c_A^{k+n} represents the current control term. c_L^{k+n} represents the limiting condition; N represents the prediction horizon; Q_ω, Q_A and Q_L represent the weighting factors. It is seen that the traditional compound cost function is complicated and contains multiple weighting factors. In order to pursue better control performance, torque and flux constraints are added into the control process. The selection process of appropriate weighting factors increases the difficulty of debugging. Therefore, an optimized parallel predictive control structure is adopted in this paper to eliminate the influence of weighting factors.

3. MODEL PREDICTION HYBRID PARALLEL DIRECT SPPED CONTROL

The block diagram of considered MP-HPDSC is shown in Fig. 2. The controller consists of the following parts: CPTC, multi-objective PPSC and LESO. The estimations of load torque and total disturbance are obtained by LESO, which has the advantages of simple structure, fast convergence and convenient parameter adjustment. Then, the torque reference required by multi-objective PPSC is obtained from CPTC. Finally, the optimal voltage vector can be selected by multi-objective PPSC.

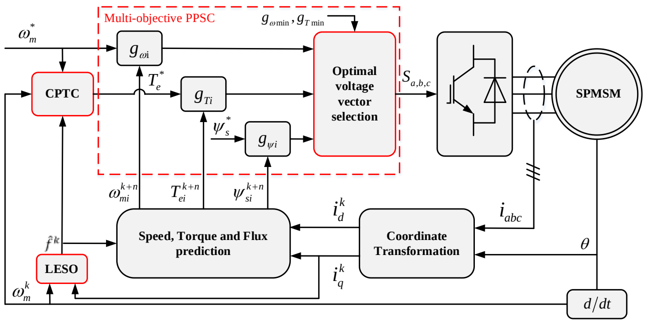

Fig. 2. Control block diagram of proposed MP-HPDSC.

From (1) to (4), the speed equation can be rewritten as:

$$\dot{\omega}_m = -\frac{B}{J}\omega_m + \frac{K_t}{J}i_q - \frac{1}{J}T_l \text{ c} \tag{7}$$

where i_q is input, ω_m is output. It should be noted that this model is established under the condition of neglecting cross-coupling magnetic saturation, structural asymmetry, iron loss, magnetic eddy current loss and harmonics.

To accomplish a precise model, all above neglected and unknown items of the system combined with T_l are covered in one variable f, and the precise model can be written as follows:

$$\dot{\omega}_m = -a_0\omega_m + d_0 i_q + f \tag{8}$$

where $a_0 = \frac{B}{J}$, $d_0 = \frac{K_t}{J}$, f includes the load torque, unknown and unmodeled parts that need to be estimated. Then, (8) can be rewritten as the following state space form:

$$\begin{aligned} \dot{x} &= Ax + Du + E\dot{f} \\ y &= Cx \end{aligned} \tag{9}$$

where $x = [x_1 \quad x_2]^T = [\omega_m \quad f]^T$, $u = i_q$, $y = \omega_m$,

$$A = \begin{bmatrix} -a_0 & 1 \\ 0 & 0 \end{bmatrix}, D = \begin{bmatrix} d_0 \\ 0 \end{bmatrix}, C = [1 \quad 0], E = [0 \quad 1]^T.$$

Then, the LESO can be designed as follow (Gao, 2015):

$$\begin{aligned} \dot{\hat{x}} &= [A - LC]\hat{x} + [D \quad L]u_c \\ y_c &= \hat{x} \end{aligned} \tag{10}$$

where $\hat{x} = [\hat{\omega}_m \quad \hat{f}]^T$ represents the estimated value of the state variable; $u_c = [u \quad y]^T$ is the combined input; y_c is the output; $L = [l_1 \quad l_2]^T$ is the gain matrix of the observer to be designed. According to (10), the characteristic polynomial of LESO can be expressed as:

$$|sI - (A - LC)| = s^2 + (a_0 + l_1)s + l_2 \tag{11}$$

It is proposed in (Gao, 2015) that make the poles of (11) both fall at the same position $(-\omega_0)$, which can reduce the parameters to be designed and satisfy the requirements of fast response. The parameters of the gain matrix are obtained as:

$$\begin{cases} l_1 = -2 * \omega_0 - a_0 \\ l_2 = \omega_0^2 \end{cases}.$$

The estimated value $\hat{f}$ can be obtained through (10), and the rotational speed equation can be rewritten as follows:

$$\dot{\omega}_m(t) = \frac{1}{J}\left(T_e(t) - \hat{f}(t) - B\omega_m(t)\right) \tag{12}$$

After discretization of the above formula by first-order Euler discretization method, the following equation can be obtained:

$$\omega_m^{k+1} = \omega_m^k + \frac{h}{J}\left(T_e^k - \hat{f}^k - B\omega_m^k\right) \tag{13}$$

where $\hat{f}^k$ represents the estimated value of f^k. According to the principle of deadbeat predictive control, the predicted speed value (ω_m^{k+1}) in (13) is equal to the reference speed (ω_m^{*k}), and the reference torque value (T_e^*) can be obtained as follows (Garcia et al., 2016; Altuna et al., 2016):

$$T_e^{*(k+1)} = \frac{J}{h}\left[\omega_m^{*k} - \left(1 - h\frac{B}{J}\right)\omega_m^k\right] + \hat{f}^k \tag{14}$$

where $T_e^{*(k+1)}$ represents the torque reference value at (k+1)th time. It should be noted that the accuracy of reference torque is affected by the load torque detection accuracy, system uncertainty and disturbance. LESO can accurately estimate the load torque with only rough parameters, and improve the robustness of the system to parameter mismatch and external disturbance (Gao, 2015).

3.2 Multi-Objective Parallel Predictive Speed Control

The constraints in the cost function of proposed MP-HPDSC are speed, torque and flux linkage. The predicted values of speed, torque and flux linkage can be obtained by (6) and (15), respectively.

$$\begin{cases} T_e^{k+1} = 1.5p\psi_f i_q^{k+1} \\ |\psi_s^{k+1}| = \sqrt{(L_s i_d^{k+1} + \psi_f)^2 + \left(L_s i_q^{k+1}\right)^2} \end{cases} \tag{15}$$

where T_e^{k+1} and $|\psi_s^{k+1}|$ are the predicted value of torque and flux linkage. Then, the independent cost functions are defined as follows:

$$\begin{cases} g_{\omega i}^{k+n} = I_{mi}^{k+n} \sum_{n=1}^{N} \left[\left| \omega_m^{*k} - \omega_{mi}^{k+n} \right| \right] \\ g_{Ti}^{k+n} = I_{mi}^{k+n} \sum_{n=1}^{N} \left[\left| T_e^{*k} - T_{ei}^{k+n} \right| \right] \\ g_{\psi i}^{k+n} = I_{mi}^{k+n} \sum_{n=1}^{N} \left[\left| |\psi_s^{*k}| - |\psi_{si}^{k+n}| \right| \right] \end{cases} \tag{16}$$

where the upper corner mark * represents the reference value; N represents the prediction horizon (N=2); I_{mi} represents the limitation of stator currents (Wu et al., 2018).

$$I_{mi}^{k+n} = \begin{cases} 1, & \left| i_{si}^{k+n} \right| \le \left| i_{s\_max} \right| \\ \infty, & \left| i_{si}^{k+n} \right| > \left| i_{s\_max} \right| \end{cases} \tag{17}$$

Different from the classification method of candidate voltage vector matrix (CVVM) in conventional PPTC (Wang et al., 2020a), the proposed MP-HPDSC discards the dynamic boundary condition and directly classifies all VVs according to the cost function value. The three VVs that minimize the values of $g_{\omega i}^{k+n}$, g_{Ti}^{k+n} and $g_{\psi i}^{k+n}$ are stored in the CVVMs (V_{OW}, V_{OT} and V_{OF}), respectively; The 3 candidate VVs can effectively guarantee the importance of the constraint condition and reflect the proportion of the constraint condition in the control process (Zhang et al., 2019b). In addition, the remaining five VVs that maximize g_{Ti}^{k+n} and $g_{\psi i}^{k+n}$ are stored in CVVMs (V_{ST} and V_{SF}) accordingly. Hence, there must be intersection between V_{OW} and any other two CVVMs. There are four possibilities for the intersection between the five CVVMs. The control flow is shown in Fig. 3.

Case1: there are common VVs among V_{OW}, V_{OT} and V_{OF}, and the VV that minimizes $g_{\omega i}^{k+n}$ is selected from the intersection set and named S1.

Case2: there are common VVs among V_{OW}, V_{OT} and V_{SF}, and the VV that minimizes $g_{\psi i}^{k+n}$ is selected from the intersection set and named S2.

Case3: there are common VVs among V_{OW}, V_{ST} and V_{OF}. In this case, if the minimum g_{Ti}^{k+n} value of these common VVs is less than the boundary condition (g_{Tmin}), the VV that minimizes g_{Ti}^{k+n} is selected as optimal VV, and decrease g_{Tmin} by 5% and named S4; Otherwise, VV that minimizes g_{Ti} is selected from all eight VVs, and increase g_{Tmin} by 5% and named S3.

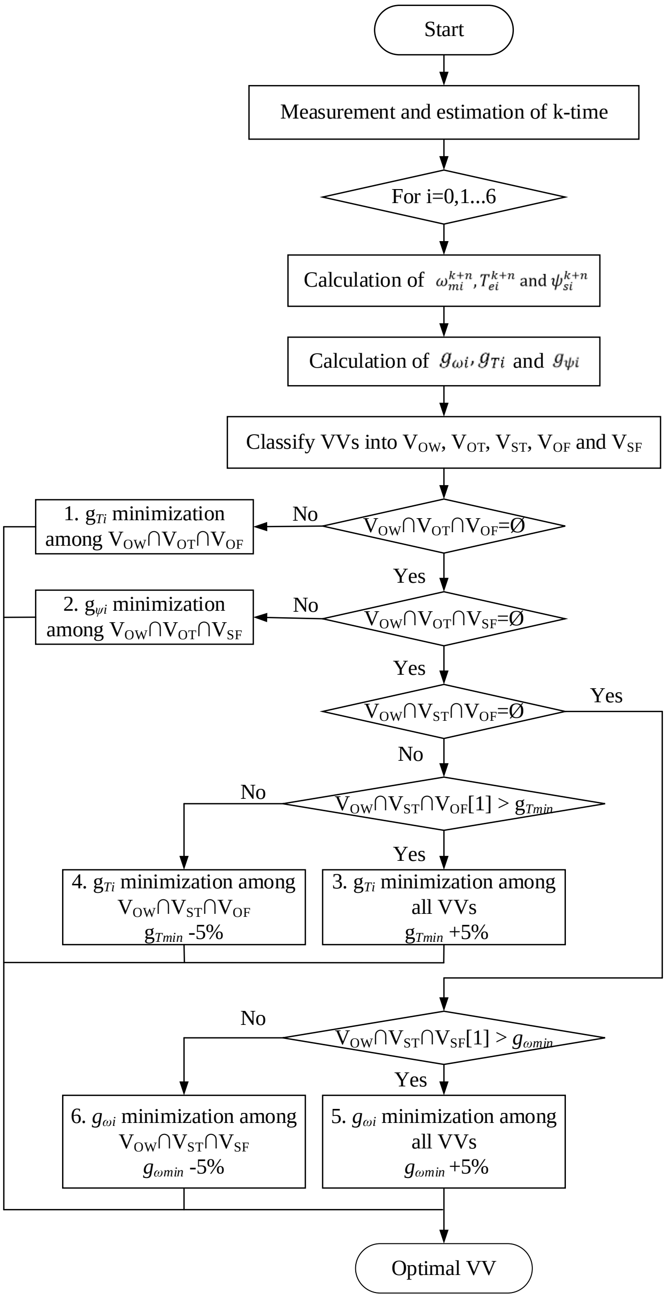

Fig. 3. The control flow of the optimized multi-objective PPSC.

Case4: there are common VVs among V_{OW}, V_{ST} and V_{SF}. In this case, if the minimum $g_{\omega i}^{k+n}$ value of these common VVs is less than the boundary condition ($g_{\omega min}$), the VV that minimizes $g_{\omega i}^{k+n}$ is selected as optimal VV, and decrease $g_{\omega min}$ by 5% and named S6; Otherwise, VV that minimizes $g_{\omega i}^{k+n}$ is selected from all eight VVs, and increase $g_{\omega min}$ by 5% and named S5.

4. SIMULATION PERFORMANCE EVALUATION

In order to verify the effectiveness of the proposed method, simulation comparisons of MP-DSC (Preindl et al., 2013), PPTC (Wang et al., 2020a) and the MP-HPDSC are performed in MATLAB/Simulink. The parameters of SPMSM are shown in Table 2. In conventional PPTC, PI controller parameter of speed control loop is $k_P = 0.3$, $k_I = 2.5$. The initial values of boundary conditions ($g_{\omega min}$ and g_{Tmin}) are 6.1r/min and 1.5N.m. The sampling period (h) is $50\mu s$.

Table 2. Machine parameters.

Parameter	Description	Value
P_N (kW)	Rated power	1
N_N (rpm)	Rated speed	1000
T_N (N.m)	Rated torque	4.5
p	Number of pole pairs	4
R_s (Ω)	Stator resistance	1.35
L_s (mH)	Stator inductance	3.17
ψ_f (Wb)	Rotor flux linkage	0.14
J (Kg·m^2)	Rotor inertia	0.64×10^{-3}
B (N.m.s)	Viscous friction coefficient	0.8×10^{-3}

4.1 Dynamic performance analysis

The simulation results of speed, torque and flux linkage of the three methods are illustrated in Fig. 4. The operating state variations and load torque estimation of MP-HPDSC are shown in Fig. 5. The speed reference rises from 100r/min to 1000r/min at 0.5s and then decreases to 100r / min at 3s with the load torque is 2N.m. Then, white noise with sample time of 0.1s was added to load torque at 1s to simulate driving conditions. In addition, ITAE is a comprehensive indicator to evaluate the performance during operation, and ITAE is defined as follow:

$$\begin{cases} ITAE_\omega = \sum_{\tau=t_1}^{t_2} \tau |e_\omega(\tau)|\, d\tau + ITAE_\omega(t_1) \\ ITAE_T = \sum_{\tau=t_1}^{t_2} \tau |e_T(\tau)|\, d\tau + ITAE_T(t_1) \end{cases}$$

where t_1 and t_2 are the evaluation intervals; $e_\omega = \omega_m^* - \omega_m$; $e_T = T_e^* - T_e$.

It is seen from Fig. 4 that the speed and torque response performance of the three methods are very similar, the performance comparisons of the three methods are shown in Table 3. Under torque dynamic conditions, PPTC has the largest speed ripple ($\Delta\omega_{max}$) at low speed and rated speed, followed by MP-DSC. On the contrary, the torque (ΔT_{emax}) and flux ($\Delta\psi_{smax}$) ripple of PPTC are less than MP-DSC. The speed, torque and flux ripple of MP-HPDSC is smallest. In Fig. 4, from 1s to 3s, the speed ITAE values of conventional MP-DSC, PPTC and MP-HPDSC are 13.48, 14.72 and 12.35, and the torque ITAE values are 5.11, 4.06 and 3.58 respectively. Hence, the simulation results confirm that MP-HPDSC has the best dynamic response performance.

It is seen from Fig. 5 that the system mainly operates in state 1-3, and the observer can quickly track the load variations. At low speed and rising speed, as shown in Fig. 5 (c)-(e), the occurrence number of states 2 and 3 is significantly higher than that of rated speed with load variations. The switching of various operating states ensures the response performance of the machine under the low-speed and speed variation.

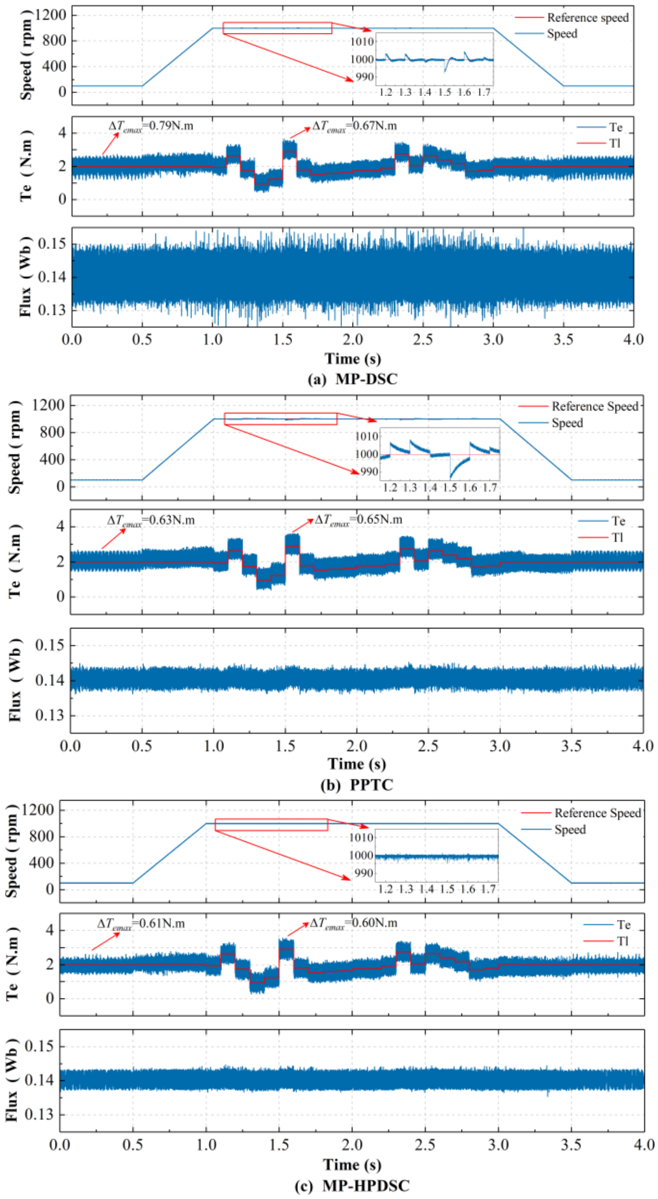

Fig. 4. The simulation results of speed, torque and flux of the three methods. (a) MP-DSC. (b) PPTC. (c) MP-HPDSC.

Table 3. Maximum ripple comparative analysis.

Condition	MP-DSC	PPTC	MP-HPDSC
$\Delta\omega_{max}$ (r/min) at 100r/min	2.6	4.7	3.4
$\Delta\omega_{max}$ (r/min) at 1000r/min	8.1	15.6	5.2
ΔT_{emax} (N.m) at 100r/min	0.79	0.63	0.61
ΔT_{emax} (N.m) at 1000r/min	0.67	0.65	0.60
$\Delta\psi_{smax}$ (Wb) at 100r/min	0.0098	0.0052	0.0044
$\Delta\psi_{smax}$ (Wb) at 1000r/min	0.0149	0.0055	0.0051

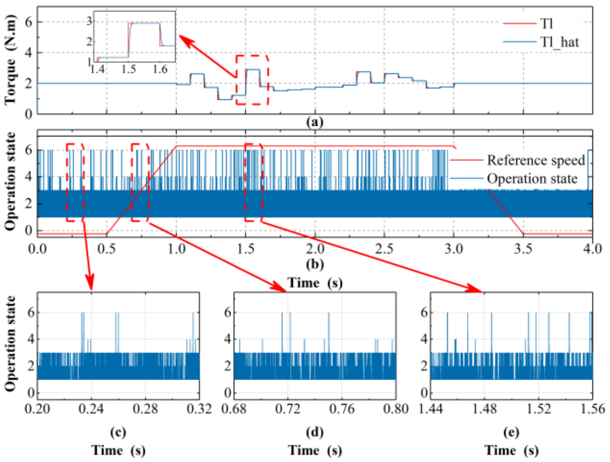

Fig. 5. Operation state and load torque estimation of MP-HPDSC. (a) Load torque estimation. (b) Operation state. (c) Operation state at 100r/min. (d) Operation state with speed rise. (e) Operation state at 1000r/min with load torque variation.

The comparisons of load torque dynamic performance of the three methods are shown in Fig. 6. Under the condition of load dynamics, the speed and torque ITAE values within 1s of the motor were evaluated at different speeds. The speed range of evaluation is 100r/min, 200r/min..., 1000r/min. Each evaluation load torque is 2N.m and accompanied by white noise with a sample time of 0.1s. Based on the simulation results in Fig. 6, the torque dynamic performance analysis among the three methods as shown in Table 4. In the range of speed variation, the speed ITAE value variation ($ITAE_{\Delta\omega}$) of PPTC was the most obvious, followed by MP-DSC. On the contrary, the torque ITAE value variation ($ITAE_{\Delta T}$) is the largest in MP-DSC, followed by PPTC. And the MP-HPDSC can show the batter response performance in both speed and torque.

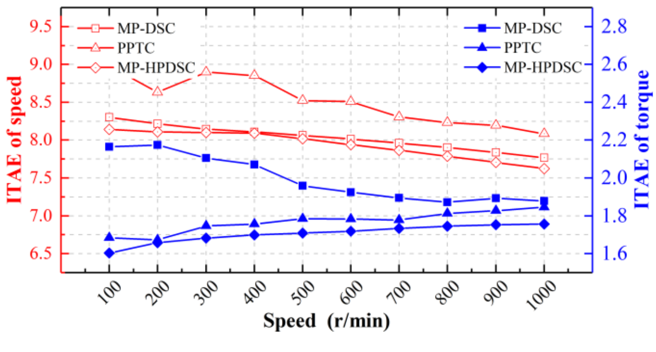

Fig. 6. ITAE values of speed and torque with speed variation form 100r/min to 1000r/min under load torque dynamic condition.

Table 4. ITAE values comparison under torque dynamics

	MP-DSC	PPTC	MP-HPDSC
$ITAE_{\Delta\omega}$	0.635	0.9	0.62
$ITAE_{\Delta T}$	0.29	0.16	0.15

4.2 Steady state performance analysis

The comparisons of steady-state performance of the three methods are shown in Fig. 7. The speed and torque ITAE values within 1s of the motor were evaluated at different speeds under rated load conditions. The speed range of evaluation is 100r/min, 200r/min..., 1000r/min. The ITAE values comparison in steady state as shown in Table 5. The maximum ITAE values variation of speed ($ITAE_{\Delta\omega}$) and torque ($ITAE_{\Delta T}$) of MP-HPDSC is still lower than that of MP-DSC and PPTC. MP-HPDSC has excellent steady-state performance in a wide speed regulation range.

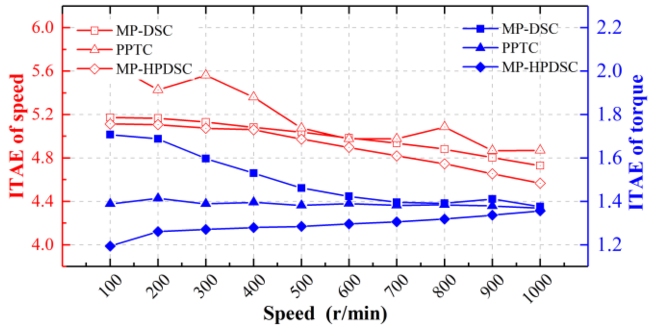

Fig. 7. ITAE values of speed and torque with speed variation from 100r/min to 1000r/min under steady state conditions.

Table 5. ITAE values comparison in steady state.

	MP-DSC	PPTC	MP-HPDSC
$ITAE_{\Delta\omega}$	0.543	0.805	0.393
$ITAE_{\Delta T}$	0.185	0.18	0.162

5. EXPERIMENTAL PERFORMANCE EVALUATION

A 1-kW SPMSM servo system experimental platform is constructed as shown in Fig. 8. The control circuit includes dSPACE/MicroLabBox, IPM (PM50CLA120) drive circuit, measurement circuit, PC and power supply (62050H-600S). The PMSM parameters are the same as those listed in Table 2. The switching frequency and related parameters of conventional MP-DSC, PPTC and proposed MP-HPDSC are consistent with the simulation section. The experimental process includes a reversal experiment to illustrate the stability of the system, the load torque step experiment and the steady-state experiment to compare the performance differences between the three control methods.

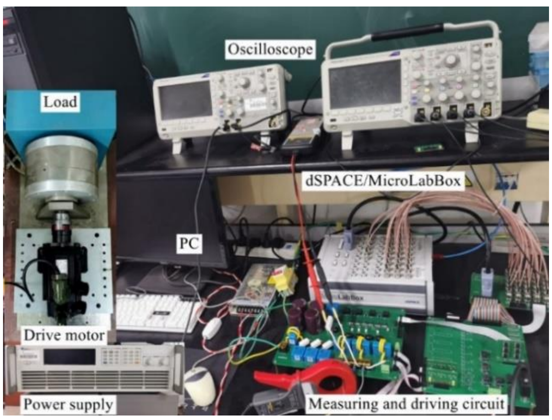

Fig. 8. Experimental platform.

5.1 Speed Reversal Performance Analysis

In order to verify the feasibility of the proposed MP-HPDSC method, the response performance of positive and negative rotation is given. The experimental results of speed, torque and flux response are shown in Fig. 9. The reference speed is reduced from 1000r/min to -1000r/min without load torque. It is seen from Fig. 9 that the speed of the machine drops from +1000r/min to -1000r/min within 0.327s, which indicates that the system is stable, and the MP-FPDSC has fast dynamic response capability in the whole speed range.

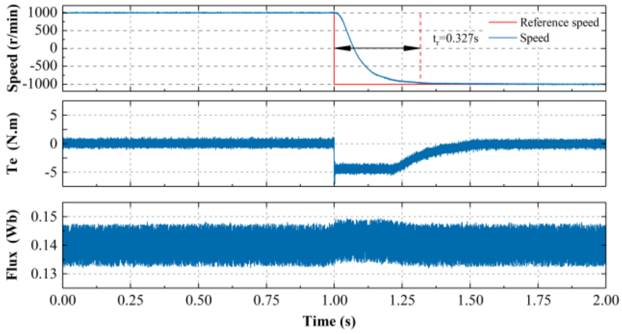

Fig. 9. The experimental results of speed, torque and flux linkage response under inversion.

5.2 Torque Step Performance Analysis

The experimental results of load torque step response performance of conventional MP-DSC, conventional PPTC and MP-HPDSC are illustrated in Fig. 10. The performance comparison under dynamic torque condition is shown in Table 6. It is seen from Table 6 that the speed response of PPTC shows the worst performance in coping with load changes. Both MP-DSC and MP-HPDSC show better robustness to load changes. MP-HPDSC has the best performance in speed overshooting and rise time. In contrast, MP-DSC has the worst torque and flux pulsation, followed by PPTC and MP-HPDSC. In general, MP-HPDSC has the best performance in dealing with external disturbances.

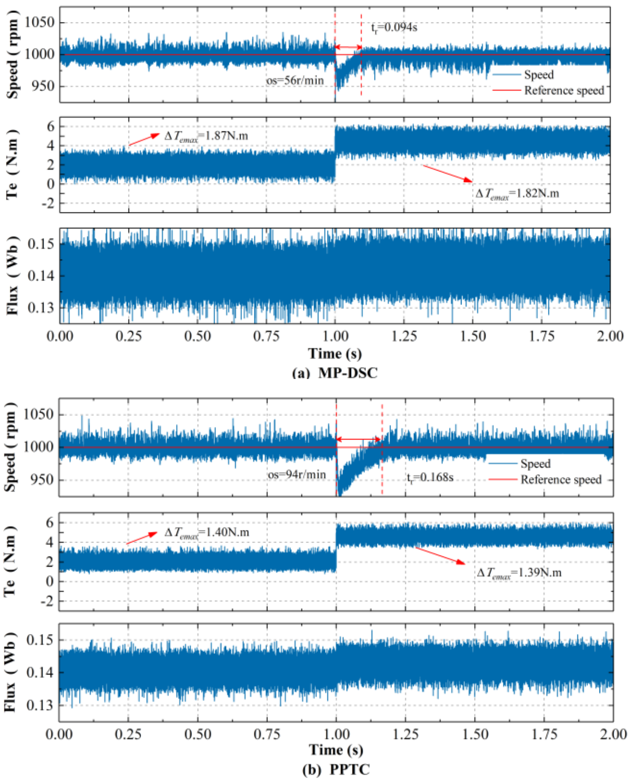

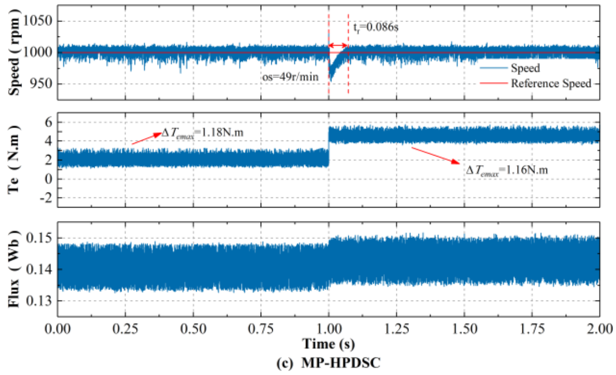

Fig. 10. Experimental results of load torque step variation under steady speed condition. (a) MP-DSC. (b) PPTC. (c) MP-HPDSC.

Table 6. Torque dynamic performance comparison.

	MP-DSC	PPTC	MP-HPDSC
Speed over-shoot (r/min)	56	94	49
Rise time (s)	0.094	0.168	0.086
Torque ripple (N.m) at low load	1.87	1.40	1.18
Torque ripple (N.m) at rated load	1.82	1.39	1.16

5.3 Steady State Performance Analysis

The comparisons of steady-state performance of the three methods are shown in Fig. 11. The speed and torque ITAE values within 1s of the motor were evaluated at different speeds under rated load conditions. The speed range of evaluation is 100r/min, 200r/min..., 1000r/min. Steady-state performance analysis is shown in Table 7. It is seen from Table 7 that the maximum ITAE values variation of speed ($ITAE_{\Delta\omega}$) and torque ($ITAE_{\Delta T}$) of MP- HPDSC is still lower than that of MP-DSC and PPTC. The experimental results are consistent with the simulation.

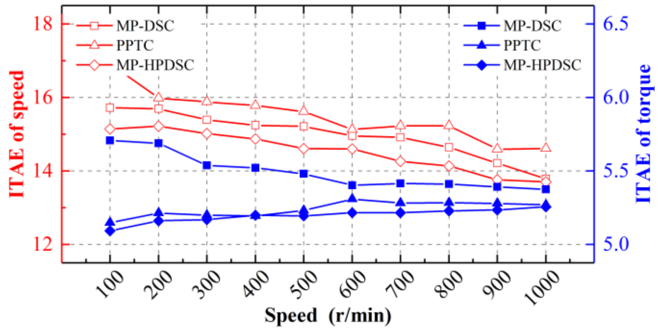

Fig. 11. Experimental results of speed and torque ITAE values under speed variation from 100r/min to 1000r/min.

Table 7. Steady-state performance comparison.

	MP-DSC	PPTC	MP-HPDSC
$ITAE_{\Delta\omega}$	1.53	2.31	1.45
$ITAE_{\Delta T}$	0.34	0.22	0.16

The THD value of stator current i_a of the three methods under speed variation are shown in Fig. 12. With the speed gradually increasing to the rated speed, the THD values all gradually decreased. MP-DSC always had the highest THD value. The highest THD values of MP-DSC, PPTC and MP-HPDSC at speed of 100r/min are 15.14%, 13.21% and 12.34% respectively. The THD values of PPTC and MP-HPDSC are similar, which are 10.34% and 10.1% at 1000 r/min, and MP-DSC is 12.83%. In conventional PPTC and MP-HPDSC methods, a parallel structure is used to balance the relationship between the constraints, so that the stator current has a smaller harmonic content. Therefore, the current THD values of MP-HPDSC and conventional PPTC are similar and both can remain stable.

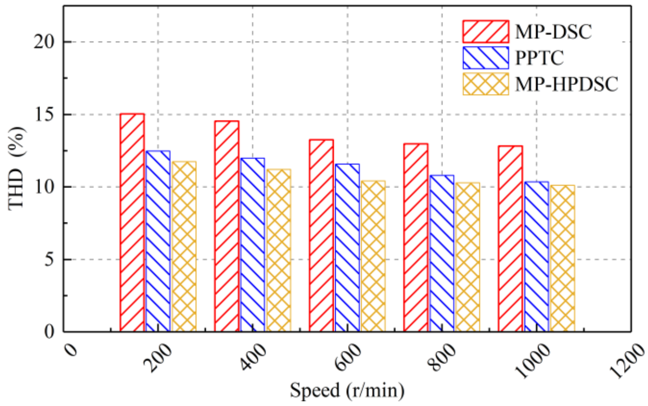

Fig. 12. Experimental results of current THD under speed variation.

The MP-HPDSC is based on LESO disturbance estimation technology, CPTC fast response ability and parallel prediction elimination weighting factor, and its performance is better than that of conventional methods. The comparison results from Table 3 to Table 7 are summarized in Table 8. This shows that MP-HPDSC method can improve the ability of fast-tracking speed and stable output torque, while maintaining flux control performance, which is more suitable for electric vehicle control system.

Table 8. Comparative issues.

Feature	MP-DSC	PPTC	MP-HPDSC
Dynamic response	Medium	Low	High
Steady response	Low	Medium	High
Anti-disturbance	Medium	Low	High
Torque ripple	High	Medium	Low
Flux ripple	High	Medium	Low

6. CONCLUSIONS

A MP-HPDSC control strategy for PMSM is proposed based on parallel prediction control in this paper. Weighting factors are eliminated and the original parallel structure is improved to optimize the cost function of speed, torque and flux linkage simultaneously. The speed tracking ability is increased. Moreover, the CPTC and LESO is introduced to improve the stability of the system.

The simulation and experimental results show that the proposed MP-HPDSC has faster speed response and stable output torque in the full speed range compared with conventional MP-DSC and PPTC. In response to load mutation, the transition time of MP-HPDSC is 83ms, which is 2/3 of MP-DSC and 1/2 of PPTC. In the whole speed range, the change of speed and torque ITAE value of MP-HPDSC ($ITAE_{\Delta\omega}$=1.45 and $ITAE_{\Delta T}$=0.16) is lower than that of conventional ($ITAE_{\Delta\omega}$=1.53 and $ITAE_{\Delta T}$=0.34) and PPTC ($ITAE_{\Delta\omega}$=2.31 and $ITAE_{\Delta T}$=0.22), showing better stability. The faster dynamic response and better stable output capability show that MP-HPDSC is suitable for electric vehicle drive system.

REFERENCES

Altuna, J. A. T., Jacomini, R. V., Puma, J. L. A., Capovilla, C. E. and Filho, A. J. S. 2016. Deadbeat controller applied to induction motor direct torque control with low-speed operation. *Electrical Engineering,* 100**,** 123-128.

Casadei, D., Profumo, F., Serra, G. and Tani, A. 2002. Foc and DTC: two viable schemes for induction motors torque control. *IEEE Transactions on Power Electronics,* 17**,** 779-787.

Caseiro, L. M. A., Mendes, A. M. S. & Cruz, S. M. A. 2019. Dynamically Weighted Optimal Switching Vector Model Predictive Control of Power Converters. *IEEE Transactions on Industrial Electronics,* 66**,** 1235-1245.

Gao, Z. 2015. Active disturbance rejection control_ From an enduring idea to an emerging technology. *2015 10th International Workshop on Robot Motion and Control (RoMoCo).* Poznan, Poland: IEEE.

Garcia, C., Silva, C., Rodriguez, J. & Zanchetta, P. 2016. Cascaded model predictive speed control of a permanent magnet synchronous machine. *IECON 2016 - 42nd Annual Conference of the IEEE Industrial Electronics Society.* Florence, Italy: IEEE.

Guazzelli, P. R. U., de Andrade Pereira, W. C., de Oliveira, C. M. R., de Castro, A. G. & de Aguiar, M. L. 2019. Weighting Factors Optimization of Predictive Torque Control of Induction Motor by Multiobjective Genetic Algorithm. *IEEE Transactions on Power Electronics,* 34**,** 6628-6638.

Huang, Z., Lin, C. & Xing, J. 2021. A Parameter-Independent Optimal Field-Weakening Control Strategy of IPMSM for Electric Vehicles Over Full Speed Range. *IEEE Transactions on Power Electronics,* 36**,** 4659-4671.

Jabbour, N. & Mademlis, C. 2019. Online Parameters Estimation and Autotuning of a Discrete-Time Model Predictive Speed Controller for Induction Motor Drives. *IEEE Transactions on Power Electronics,* 34**,** 1548-1559.

Li, L. & Liu, Q. 2019. Research on IPMSM Drive System Control Technology for Electric Vehicle Energy Consumption. *IEEE Access,* 7**,** 186201-186210.

Liu, X., Chen, H., Zhao, J. & Belahcen, A. 2016. Research on the Performances and Parameters of Interior PMSM Used for Electric Vehicles. *IEEE Transactions on Industrial Electronics,* 63**,** 3533-3545.

Mwasilu, F., Nguyen, H. T., Choi, H. H. & Jung, J.-W. 2017. Finite Set Model Predictive Control of Interior PM Synchronous Motor Drives With an External Disturbance Rejection Technique. *IEEE/ASME Transactions on Mechatronics*, 22**,** 762-773.

Navardi, M. J., Milimonfared, J. & Talebi, H. A. 2018. Torque and Flux Ripples Minimization of Permanent Magnet Synchronous Motor by a Predictive-Based Hybrid Direct Torque Control. *IEEE Journal of Emerging and Selected Topics in Power Electronics*, 6**,** 1662-1670.

Preindl, M. & Bolognani, S. 2013. Model Predictive Direct Speed Control with Finite Control Set of PMSM Drive Systems. *IEEE Transactions on Power Electronics*, 28**,** 1007-1015.

Rodriguez, J. & Cortes, P. (2012). 133-144. *Predictive Control of Power Converters and Electrical Drives,* John Wiley & Sons, Chichedter, U.K.

Sun, X., Yu, H., Yu, J. & Liu, X. 2019. Design and implementation of a novel adaptive backstepping control scheme for a PMSM with unknown load torque. *IET Electric Power Applications*, 13**,** 445-455.

Uddin, M. N. & Rahman, M. M. 2019. Online Torque-Flux Estimation-Based Nonlinear Torque and Flux Control Scheme of IPMSM Drive for Reduced Torque Ripples. *IEEE Transactions on Power Electronics*, 34**,** 636-645.

Vafamand, N., Arefi, M. M., Khooban, M. H., Dragicevic, T. & Blaabjerg, F. 2019. Nonlinear Model Predictive Speed Control of Electric Vehicles Represented by Linear Parameter Varying Models With Bias Terms. *IEEE Journal of Emerging and Selected Topics in Power Electronics,* 7**,** 2081-2089.

Wakodikar, A. & Aware, M. V. 2020. Speed Sensorless Finite Set Model Predictive Speed Control of Induction Motor. *2020 IEEE First International Conference on Smart Technologies for Power, Energy and Control (STPEC).* Nagpur, India: IEEE.

Wang, F., Xie, H., Chen, Q., Davari, S. A., Rodriguez, J. & Kennel, R. 2020a. Parallel Predictive Torque Control for Induction Machines Without Weighting Factors. *IEEE Transactions on Power Electronics*, 35**,** 1779-1788.

Wang, F., Zuo, K., Lin, G., He, L., Rodriguez, J. & Garcia, C. 2020b. Adaptive Stator Current Disturbance Observer based on the Predictive Current Control for PMSM. *IECON 2020 The 46th Annual Conference of the IEEE Industrial Electronics Society.* Singapore: IEEE.

Wu, X., Song, W. & Xue, C. 2018. Low-Complexity Model Predictive Torque Control Method Without Weighting Factor for Five-Phase PMSM Based on Hysteresis Comparators. *IEEE Journal of Emerging and Selected Topics in Power Electronics,* 6**,** 1650-1661.

Xie, H., Wang, F., He, Y., Rodriguez, J. & Kennel, R. 2021. Encoderless Parallel Predictive Torque Control for Induction Machine Using A Robust Model Reference Adaptive System. *IEEE Transactions on Energy Conversion***,** 1-1.

Xie, H., Xun, Q., Tang, Y., Wang, F., Rodriguez, J. & KENNEL, R. 2020. Robust Parallel Predictive Torque Control with Model Reference Adaptive Estimator for IM Drives. *2020 International Conference on Electrical Machines (ICEM).* Gothenburg, Sweden: IEEE.

Zhang, X. & He, Y. 2019a. Direct Voltage-Selection Based Model Predictive Direct Speed Control for PMSM Drives Without Weighting Factor. *IEEE Transactions on Power Electronics,* 34**,** 7838-7851.

Zhang, Y. & Yang, H. 2015. Generalized Two-Vector-Based Model-Predictive Torque Control of Induction Motor Drives. *IEEE Transactions on Power Electronics,* 30**,** 3818-3829.

Zhang, Y., Yang, H. & Xia, B. 2016. Model-Predictive Control of Induction Motor Drives: Torque Control Versus Flux Control. *IEEE Transactions on Industry Applications,* 52**,** 4050-4060.

Zhang, Y., Zhang, B., Yang, H., Norambuena, M. & Rodriguez, J. 2019b. Generalized Sequential Model Predictive Control of IM Drives With Field-Weakening Ability. *IEEE Transactions on Power Electronics,* 34**,** 8944-8955.